Orientation effects on evaporation residue cross sections in ^{48}Ca-induced hot fusion reactions

Long Zhu,[1,2,*] Zhao-Qing Feng,[3,†] Cheng Li,[1,2] and Feng-Shou Zhang[1,2,4,‡]

[1]*The Key Laboratory of Beam Technology and Material Modification of Ministry of Education, College of Nuclear Science and Technology, Beijing Normal University, Beijing 100875, China*

[2]*Beijing Radiation Center, Beijing 100875, China*

[3]*Institute of Modern Physics, Chinese Academy of Sciences, Lanzhou 730000, China*

[4]*Center of Theoretical Nuclear Physics, National Laboratory of Heavy Ion Accelerator of Lanzhou, Lanzhou 730000, China*

(Received 20 June 2014; published 24 July 2014)

Within the framework of the dinuclear system model, the evaporation residue (ER) cross sections of superheavy nuclei in ^{48}Ca-induced hot fusion reactions with different entrance orientations are investigated. The production cross sections are obtained by calculating the average ER cross sections for different orientations of deformed colliding nuclei. The average results are in good agreement with the experimental data. The orientation effects on ER cross sections are investigated through studying the orientation dependence of the capture cross sections and the fusion probability. It is found that the fusion probabilities with the polar orientation of the target are higher than those with the equatorial orientation at lower incident energies, while the opposite behavior can be seen at high incident energy regions. The production cross sections for synthesizing $Z = 119$ and 120 by fusion reactions of ^{48}Ca with actinide targets are predicted.

DOI: 10.1103/PhysRevC.90.014612 PACS number(s): 25.70.Mn, 25.70.Pq, 24.10.Lx

I. INTRODUCTION

In recent years, much progress has been made in synthesis of superheavy nuclei (SHN) experimentally and theoretically. The SHN with $Z = 102$–118 has been synthesized by using cold fusion reactions with the targets of ^{208}Pb and ^{209}Bi [1,2] and ^{48}Ca-induced hot fusion reactions [3–10]. A lot of theoretical works have been done to investigate the synthesis mechanism of SHN [11–30].

Collisions between the deformed, oriented nuclei have been of much interest from time to time. The orientation effects have received particular attention for the formation of SHN [12,14,31,32]. Generally speaking, the process of synthesis of SHN can be divided into three steps. First, two colliding nuclei overcome the fusion barrier and form a dinuclear system. For a fusion reaction with deformed nuclei, the Coulomb barrier is lower with the pole-to-pole colliding orientation than that with the side-to-side one [33]. Therefore, it is easier to overcome the Coulomb barrier for the pole-to-pole orientation. The second step is that the dinuclear system fuses to a compound nucleus. In this step, the quasifission (QF) channels compete with the complete fusion, which strongly hinders the formation of the compound nucleus. For the deformed collision systems, the fusion probabilities are connected with the collision orientation. Some works [31,34] show that the fusion probability of equatorial orientation is higher than that of polar orientation because of the more compact configuration. In the last step, the excited compound nucleus loses its energy by the emission of particles and γ rays to reach its ground state. This step is described by using a statistical model.

The evaporation residue (ER) cross sections of SHN are usually written as a sum over all partial waves J:

$$\sigma_{\mathrm{ER}}(E_{\mathrm{c.m.}}) = \frac{\pi\hbar^2}{2\mu E_{\mathrm{c.m.}}} \sum_J (2J+1) T(E_{\mathrm{c.m.}}, J) \times P_{\mathrm{CN}}(E_{\mathrm{c.m.}}, J) W_{\mathrm{sur}}(E_{\mathrm{c.m.}}, J). \quad (1)$$

Here, $T(E_{\mathrm{c.m.}}, J)$ is the probability of the colliding nuclei overcoming the potential barrier in the entrance channel, $P_{\mathrm{CN}}(E_{\mathrm{c.m.}}, J)$ is the fusion probability, $W_{\mathrm{sur}}(E_{\mathrm{c.m.}}, J)$ is the survival probability of the compound nucleus, and $E_{\mathrm{c.m.}}$ is the bombarding energy in the center-of-mass system.

Inspired by abundant experimental data, many approaches [11,14–20] are used to study the process of synthesizing SHN. The dinuclear system (DNS) model has been successfully used in investigating the mechanism of the synthesis of SHN [11,23–29]. In most of the works the deformed nuclei are treated only in the pole-to-pole orientation. It is desirable to investigate the orientation effects of ER cross sections in the framework of the DNS model.

In this work, within the framework of the DNS model, we calculate the average ER cross sections for different orientations in hot fusion reactions and compare them with the experimental data. The orientation effects on the capture cross section and the fusion probability in the reaction ^{48}Ca + ^{238}U are studied. These effects play an essential role in the ^{48}Ca + actinide reactions. The ER cross sections for synthesizing $Z = 119$ and 120 in ^{48}Ca-induced hot fusion reactions with different collision orientations are calculated.

The article is organized as follows. In Sec. II, we describe the method of calculating ER cross sections. The results and discussion are presented in Sec. III. We summarize the main results in Sec. IV.

*zhulong@mail.bnu.edu.cn

†fengzhq@impcas.ac.cn

‡Corresponding author: fszhang@bnu.edu.cn

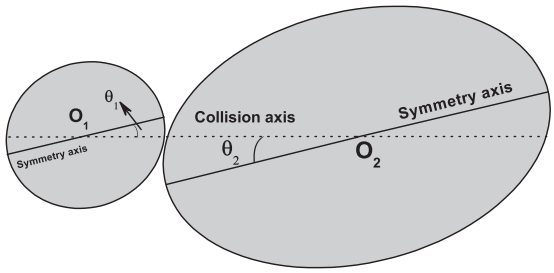

FIG. 1. Fusionlike shape parametrization for two ellipsoidal nuclei.

II. MODEL DESCRIPTION

In fusion reactions involving deformed nuclei, the ER cross sections can be written as

$$\sigma_{\rm ER}(E_{\rm c.m.}) = \frac{\pi\hbar^2}{2\mu E_{\rm c.m.}} \int_0^{\pi/2} \sin\theta_1 d\theta_1 \int_0^{\pi/2} \sum_J (2J+1) \times T(E_{\rm c.m.},J,\theta_1,\theta_2) P_{\rm CN}(E_{\rm c.m.},J,\theta_1,\theta_2) \times W_{\rm sur}(E_{\rm c.m.},J)\sin\theta_2 d\theta_2, \quad (2)$$

where θ_1 and θ_2 are the angles between the symmetry axes of the projectile (light fragment) and the target (heavy fragment) and the collision axis, respectively. The detailed description of the typical fusionlike configuration of ellipsoidal target and projectile nuclei can be seen in Fig. 1. In this work, we take the quantum number of the maximal angular momentum as $J_{\rm max} = 40$, because the fission barrier of the heavy nucleus disappears at high spin, which leads to an exponential decrease of the survival probability [35].

A. Capture cross section and transmission probability

In fusion reactions with deformed nuclei, the fusion barrier distribution is dominated by orientation effects [33,36]. Therefore, the capture cross sections can be calculated with the method described in Ref. [33]:

$$\sigma_{\rm cap}(E_{\rm c.m.}) = \frac{\pi\hbar^2}{2\mu E_{\rm c.m.}} \sum_J (2J+1) \int_0^{\pi/2} \int_0^{\pi/2} \times T(E_{\rm c.m.},\theta_1,\theta_2,J)\sin\theta_1\sin\theta_2 d\theta_1 d\theta_2. \quad (3)$$

The transmission probability can be written as

$$T(E_{\rm c.m.},\theta_1,\theta_2,J) = \frac{1}{1+\exp\left\{-\frac{2\pi}{\hbar\omega(\theta_1,\theta_2,J)}\left[E_{\rm c.m.} - B(\theta_1,\theta_2) - \frac{\hbar^2}{2\mu R_B^2(\theta_1,\theta_2,J)}\right]\right\}}, \quad (4)$$

where $\hbar\omega(\theta_1,\theta_2,J)$ is the width of the parabolic barrier and $R_B(\theta_1,\theta_2,J)$ defines a position of the barrier. The nucleus-nucleus interaction potential with quadrupole deformation is taken as the form

$$V(r,\theta_1,\theta_2) = V_N(r,\theta_1,\theta_2) + V_C(r,\theta_1,\theta_2). \quad (5)$$

The nuclear potential and Coulomb potential are taken as the forms in Ref. [37]:

$$V_N(r,\theta_1,\theta_2) = -V_0 \left\{1+\exp\left[\left(r - \sum_{i=1}^{2} R_i\left[1+(5/4\pi)^{1/2} \times \beta_2^{(i)} P_2(\cos\theta_i)\right]\right) a^{-1}\right]\right\}^{-1} \quad (6)$$

and

$$V_C(r,\theta_1,\theta_2) = \frac{Z_1 Z_2 e^2}{r} + \left(\frac{9}{20\pi}\right)^{1/2}\left(\frac{Z_1 Z_2 e^2}{r^3}\right) \times \sum_{i=1}^{2} R_i^2 \beta_2^{(i)} P_2(\cos\theta_i) + \left(\frac{3}{7\pi}\right)\left(\frac{Z_1 Z_2 e^2}{r^3}\right) \times \sum_{i=1}^{2} R_i^2\left[\beta_2^{(i)} P_2(\cos\theta_i)\right]^2. \quad (7)$$

Here θ_i is the angle between the symmetry axis of the ith nucleus and the collision axis. $\beta_2^{(i)}$ and R_i are quadrupole deformation parameter and the radius of the ith nucleus, respectively. The strength V_0 and the diffusion width a of the nuclear potential are set to be 80.0 MeV and 0.7 fm, respectively. The quadrupole deformation parameter is taken from Ref. [38].

B. Fusion probability

We use the DNS model to investigate the fusion process and calculate the fusion probability of SHN. In the DNS concept, the nucleon transfer process usually takes place at the bottom of potential pocket after capture of the colliding nuclei. The diffusion process is treated along proton and neutron degrees of freedom. The distribution probability is obtained by solving a set of master equations in the potential energy surface (PES) of the DNS. The time evolution of the mass asymmetry is described by the following master equation:

$$\frac{dP(Z_1,N_1,E_1,\theta_1,\theta_2,t)}{dt} = \sum_{Z_1'} W_{Z_1,N_1;Z_1',N_1}(t)\left[d_{Z_1,N_1}P(Z_1',N_1,E_1',\theta_1,\theta_2,t) - d_{Z_1',N_1}P(Z_1,N_1,E_1,\theta_1,\theta_2,t)\right] + \sum_{N_1'} W_{Z_1,N_1;Z_1,N_1'}(t)\left[d_{Z_1,N_1}P(Z_1,N_1',E_1',\theta_1,\theta_2,t) - d_{Z_1,N_1'}P(Z_1,N_1,E_1,\theta_1,\theta_2,t)\right] - \{\Lambda_{\rm QF}[\Theta(t),\theta_1,\theta_2] + \Lambda_{\rm fis}[\Theta(t)]\}P(Z_1,N_1,E_1,\theta_1,\theta_2,t). \quad (8)$$

Here $P(Z_1,N_1,E_1,\theta_1,\theta_2,t)$ is the probability distribution function to find fragment 1 with proton number Z_1 and neutron number N_1 with the corresponding local excitation energy E_1 and the contact orientation of light fragment θ_1 and heavy fragment θ_2 at time t. $W_{Z_1,N_1;Z_1',N_1} = W_{Z_1,N_1;Z_1,N_1'}$ is the mean transition probability from the channel (Z_1, N_1, E_1) to (Z_1',

N_1, $E_1^{'}$) [or (Z_1, N_1, E_1) to (Z_1, $N_1^{'}$, $E_1^{'}$)]. d_{Z_1,N_1} denotes the microscopic dimension corresponding to the macroscopic state (Z_1, N_1, E_1). The sum is taken over all possible proton and neutron numbers that fragments $Z_1^{'}$ and $N_1^{'}$ may take, but only one nucleon transfer is considered in the model.

The evolution of the DNS along the relative distance R leads to QF of the DNS. The QF rate $\Lambda_{\rm QF}[\Theta(t),\theta_1,\theta_2]$ can be treated with the one-dimensional Kramers rate [24]:

$$\Lambda_{\rm QF}[\Theta(t),\theta_1,\theta_2] = \frac{\omega}{2\pi\omega^{B_{\rm QF}}}\left[\sqrt{\left(\frac{\Gamma}{2\hbar}\right)^2+(\omega^{B_{\rm QF}})^2}-\frac{\Gamma}{2\hbar}\right] \times \exp\left[-\frac{B_{\rm QF}(Z_1,N_1,\theta_1,\theta_2)}{\Theta(t)}\right]. \quad (9)$$

The QF rate exponentially depends on the QF barrier $B_{\rm QF}(Z_1,N_1,\theta_1,\theta_2)$. The local temperature $\Theta(t)$ is calculated by using the Fermi-gas expression $\Theta=\sqrt{\varepsilon^*/a}$ with the local excitation energy ε^* and the level-density parameter $a = A/12$ MeV^{-1}. The frequency $\omega^{B_{\rm QF}}$ of the inverted harmonic oscillator approximates the potential V in R at the top of the quasifission barrier, and ω is the frequency of the harmonic oscillator approximating the potential in R around the bottom of the pocket. The Γ determines the friction coefficients. Here, $\Gamma = 2.8$ MeV, $\hbar\omega^{B_{\rm QF}} = 2.0$ MeV, and $\hbar\omega = 3.0$ MeV. The local excitation energy is defined as

$$\varepsilon^* = E_{\rm diss} - [U(A_1,\theta_1,\theta_2,J) - U(A_p,\theta_1,\theta_2,J)] - \frac{(J-M)^2}{2\zeta_{\rm rel}(\theta_1,\theta_2)} - \frac{M^2}{2\zeta_{\rm int}}. \quad (10)$$

Here, $U(A_1)$ and $U(A_p)$ are the driving potentials of fragment A_1 and the entrance point of the DNS and where the orientation effects are considered. $E_{\rm diss}$ is the excitation energy of the composite system, which is converted from the relative kinetic energy loss. $E_{\rm diss}$ is related to the incident energy and to the minimum of the well bottom of the nucleus-nucleus potential $V(R_m)$ as shown in Fig. 2 [11,39]. M denotes the intrinsic angular momentum derived from the dissipation of the relative angular momentum, and $\zeta_{\rm int}$ is the corresponding moment of inertia. J denotes the initial angular momentum. $\zeta_{\rm rel}$ is the relative moment of inertia of the DNS, which is given by $\zeta_{\rm rel}(\theta_1,\theta_2) = \mu R_m^2(\theta_1,\theta_2)$.

In the relaxation process of the relative motion, the relative kinetic energy is dissipated into the DNS system. The excitation energy of the composite system and the PES determines the local excitation energy. The PES of the DNS is given by

$$U(A_1,A_2,R,\beta_1,\beta_2,\theta_1,\theta_2,J) = U_{\rm LD}(A_1)+U_{\rm LD}(A_2)-U_{\rm LD}(A) + V_{\rm CN}(A_1,A_2,R,\beta_1,\beta_2,\theta_1,\theta_2,J). \quad (11)$$

$U_{\rm LD}(A_1)$, $U_{\rm LD}(A_2)$, and $U_{\rm LD}(A)$ are the binding energies of the fragments A_i and the compound nucleus A, respectively. $V_{\rm CN}$ is the interaction potential of two fragments, which depends on the deformation parameter and the orientation of the deformed fragments. The details of $V_{\rm CN}$ are given in Ref. [22]. Because the nucleon transfer process takes place at the bottom of the potential pocket, we consider only the mass asymmetry degree of freedom of the PES, which is defined as $\eta = (A_1 - A_2)/(A_1 + A_2)$.

Considering the orientation effects, the fusion probability is expressed as follows:

$$P_{\rm CN}(E_{\rm c.m.},J,\theta_1,\theta_2) = \sum_{A_1=1}^{A_{\rm BG}} P(A_1,E_{\rm c.m.},J,\theta_1,\theta_2), \quad (12)$$

where $A_{\rm BG}$ is the mass number of light fragment at the Businaro-Gallone (BG) point as shown in Fig. 3(a). In the

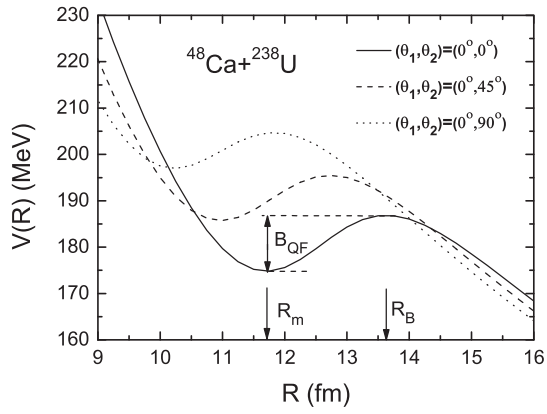

FIG. 2. The interaction potentials in the entrance channel as a function of relative distance with different colliding orientations of the target for the reaction ^{48}Ca + ^{238}U. The minimum value of the potential well is at $R = R_m$. Potential well depth $B_{\rm QF}$ is used as a quasifission barrier. The position of the barrier is denoted by R_B.

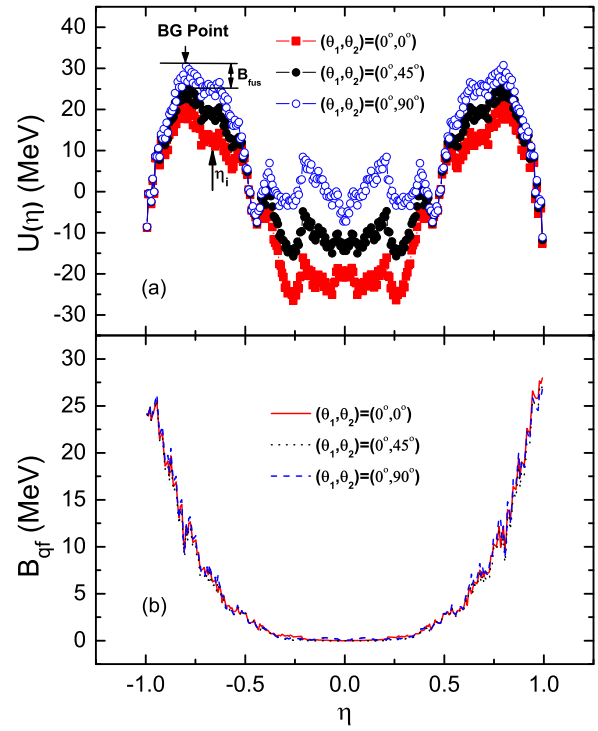

FIG. 3. (Color online) The driving potential (a) and the QF barrier (b) of DNS for the reaction ^{48}Ca + ^{238}U as a function of the mass asymmetry η at different orientations of heavy fragment θ_2.

DNS model, the fusion probability strongly depends on the excitation of composite system $E_{\rm diss}$, the QF barrier $B_{\rm QF}$, and inner fusion barrier $B_{\rm fus}$. Therefore, orientation effects on $P_{\rm CN}$ can be investigated through studying $E_{\rm diss}$, $B_{\rm QF}$, and $B_{\rm fus}$.

C. Survival probability of the excited compound nucleus

The excited compound nucleus usually loses its energy by the emission of light particles, fission, and γ rays. The emission of light charged particles and γ rays is disregarded in the model [26]. The survival probability of emitting x neutrons can be written as

$$W_{\rm sur}(E^*_{\rm CN},x,J) = P(E^*_{\rm CN},x,J)\prod_i^x\left[\frac{\Gamma_n(E^*_i,J)}{\Gamma_n(E^*_i,J)+\Gamma_f(E^*_i,J)}\right]. \quad (13)$$

Here, $E^*_{\rm CN}$ and J are the excitation energy and the spin of the compound nucleus, respectively. $E^*_{\rm CN} = E_{\rm c.m.} + Q$, where $Q = M(P)c^2 + M(T)c^2 - M(C)c^2$; and $M(P)$, $M(T)$, and $M(C)$ are the nuclear masses of the projectile, the target, and the compound nucleus, respectively. E^*_i is the excitation energy before evaporation of the ith neutron, which can be calculated from the equation

$$E^*_{i+1} = E^*_i - B^n_i - 2T_i, \quad (14)$$

with the initial condition $E^*_1 = E^*_{\rm CN}$. B^n_i is the separation energy of the ith neutron. The detailed description of the width of the ith neutron emission, the fission, and the realization probability $P(E^*_{\rm CN},x,J)$ can be found in Ref. [26]. In this work, the fission barrier before evaporating the ith neutron is obtained by

$$B^f_i(E^*_i) = B^f(E^*_i = 0)\exp(-E^*_i/E_d). \quad (15)$$

The shell correction energy $B^f(E^*_i = 0)$ is taken from Ref. [38]. $E_d = 5.48A^{1/3}/(1+1.3A^{-1/3})$ is the damping energy.

III. RESULTS AND DISCUSSION

It is reasonable to consider different colliding orientations of deformed nuclei and compare the average results with experimental data. In the DNS model, the compound nucleus is formed when all nucleons of the projectile (the light fragment) transfer into the target (the heavy fragment). In this process, the orientation effects are mainly caused by the heavy fragment, especially for ^{48}Ca-induced hot fusion reactions. Therefore, in this work we study the orientation effects through different orientations of the heavy fragment, which is described by θ_2. The orientation of the light fragment θ_1 is set to be 0°.

A. Orientation effects on ER cross sections in the reaction ^{48}Ca + ^{238}U

In Fig. 2 we present the interaction potentials in the entrance channel for the reaction ^{48}Ca + ^{238}U with $\theta_2 = 0°$, 45°, and 90°, which are calculated using Eq. (5). The QF barrier $B_{\rm QF}$ is also shown, which is described by the depth of the potential pocket. One can see that the fusion barrier for $\theta_2 = 90°$ is much higher than that for 0°. Therefore, it is easier for two colliding nuclei to overcome the fusion barrier at the polar orientation of ^{238}U.

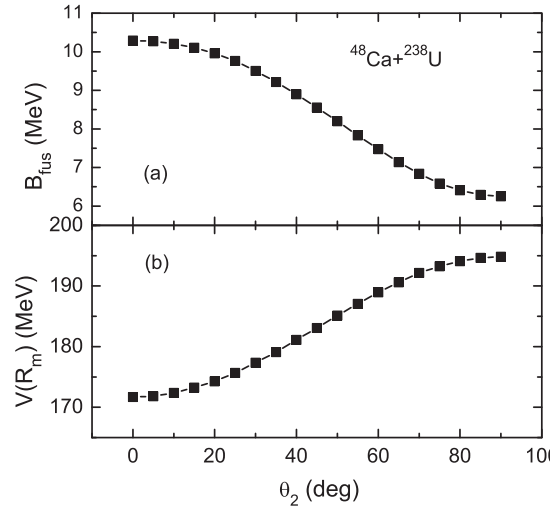

FIG. 4. The value of the inner fusion barrier $B_{\rm fus}$ (a) and nucleus-nucleus potential at the minimum of the potential pocket $V(R_m)$ (b) as a function of θ_2 for the reaction ^{48}Ca + ^{238}U.

Figure 3(a) shows the PES in the reaction ^{48}Ca + ^{238}U as a function of the mass asymmetry degrees of freedom for different values of θ_2. It can be seen that $U(\eta)$ increases with the increasing value of θ_2. Here, we consider only the left part of the PES. The $U(\eta)$ is quite close for different orientations in the vicinity of $\eta = -0.45$. This is because the static deformation of the heavy fragments in this area is quite small. The inner fusion barrier $B_{\rm fus}$ and the initial mass asymmetry $\eta_{\rm i}$ are also shown. The QF barriers as a function of η for different orientations are presented in Fig. 3(b). The results for these three cases are quite close. Hence, it can be concluded that the QF barrier does not influence the orientation effects on the fusion probability greatly.

To clarify the influence of θ_2 on the inner fusion barrier, the dependence of $B_{\rm fus}$ on θ_2 for the reaction ^{48}Ca + ^{238}U is shown in Fig. 4(a). It can be seen that $B_{\rm fus}$ decreases with the increasing value of θ_2. This fact leads to a strong increase of hindrance for the polar orientation of the ^{238}U nucleus in collision. Figure 4(b) shows the nucleus-nucleus interaction potential at the bottom of the potential pocket $V(R_m)$ as a function of θ_2. The value of $V(R_m)$ increases drastically by increasing the value of θ_2. At the same bombarding energy, the excitation energy of the DNS is larger for the lower $V(R_m)$, which leads to an increase of the fusion probability [11].

Figure 5(a) shows the comparison of calculated capture cross sections with the experimental data for the ^{48}Ca + ^{238}U reaction. The average results are in good agreement with the experimental data [40]. The capture cross sections for $\theta_2 = 0°$, 45°, and 90° are also shown. It can be seen that the curve of the capture cross section for $\theta_2 = 0°$ is much higher than that for $\theta_2 = 90°$ because of the lower Coulomb barrier for $\theta_2 = 0°$ as shown in Fig. 2. In Fig. 5(b) the fusion probabilities as a function of the excitation energy ($J = 0$) for $\theta_2 = 0°$, 45°, and 90° in the reaction ^{48}Ca + ^{238}U are shown. We notice that, for

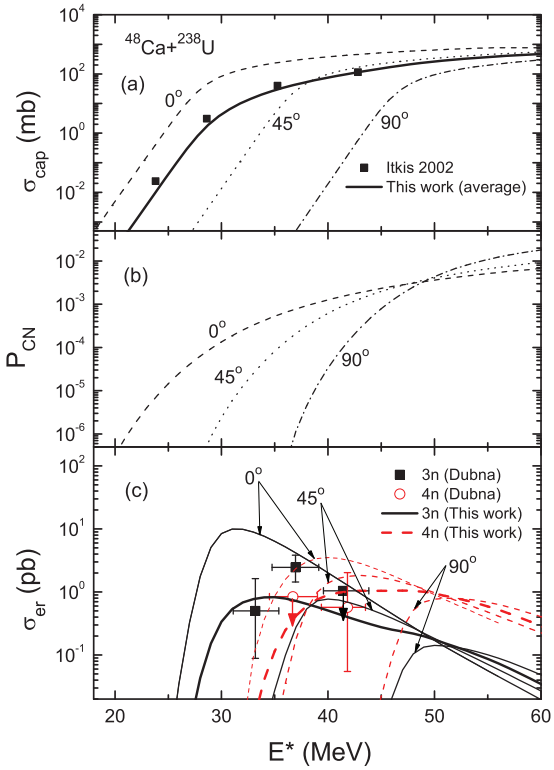

FIG. 5. (Color online) (a) Capture cross sections for the reaction ^{48}Ca + ^{238}U. The capture cross sections for $\theta_2 = 0°$, 45°, and 90° are denoted by dashed, dotted, and dot-dashed lines, respectively. The experimental data [40] are denoted by solid squares. (b) Dependence of the fusion probabilities on excitation energies ($J = 0$) for different θ_2 in the reaction ^{48}Ca + ^{238}U. (c) ER cross sections for the reaction ^{48}Ca + ^{238}U. The solid lines and the dashed lines denote the calculated ER cross sections of the $3n$ and the $4n$ channels, respectively. The thick solid and dashed lines denote the averaged results. The experimental data [6] of the $3n$ and the $4n$ channels are denoted by solid squares and circles, respectively.

lower incident energies, the fusion probabilities with the polar orientation of ^{238}U ($\theta_2 = 0°$) are higher than those with the equatorial orientation of ^{238}U ($\theta_2 = 90°$), while the opposite behavior can be seen for the high excitation energy region ($E^* > 48$ MeV). As mentioned above, the influence of $B_{\rm fus}$, $B_{\rm QF}$, and $V(R_m)$ on the competition between complete fusion and QF is strong. $B_{\rm QF}$ is not the main factor that influences the orientation effects of the fusion probability because of the small variation of the QF barrier for different orientations, as shown in Fig 3(b). Therefore, the orientation effects of the fusion probability are mainly due to the competition between $B_{\rm fus}$ and $V(R_{\rm m})$. The dependence of $B_{\rm fus}$ and $V(R_m)$ on θ_2 is shown in Fig 4. $B_{\rm fus}$ plays a leading role in the high incident energy region, which causes larger values of $P_{\rm CN}$ for $\theta_2 = 90°$. On the other hand, the orientation effects of the probability are mainly influenced by $V(R_m)$ at lower incident energies.

We assume the angles between the symmetry axes of nuclei and the collision axis are stable from the capture process to the formation of the compound nucleus. Therefore, the ER cross sections for each value of θ_2 can be calculated, as shown in Fig. 5(c), for the reaction ^{48}Ca + ^{238}U. The solid

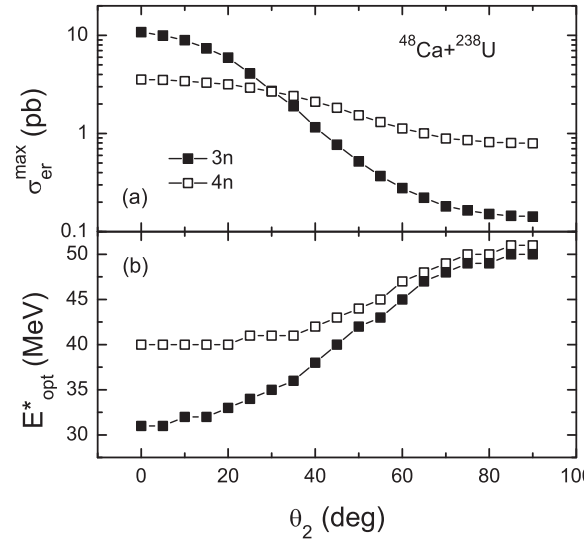

FIG. 6. The maximal values of calculated ER cross sections (a) and the optimal excitation energies (b) as a function of θ_2 in the $3n$ and the $4n$ channels in the reaction ^{48}Ca + ^{238}U.

and the dashed lines denote the ER cross sections of the $3n$ and the $4n$ channels, respectively. The thick lines represent the average results. Within the error bars, the experimental data are reproduced rather well. The ER cross section of the $3n$ channel for $\theta_2 = 0°$ is quite high and the corresponding optimal excitation energy is low in comparison to the curve for $\theta_2 = 90°$. The possible reason for that is the rather high capture cross section for the polar orientation of the ^{238}U nucleus, especially in the sub-barrier region, as shown in Fig. 5(a).

The next step in studying the orientation effects of ER cross sections is to study the maximal ER cross section $\sigma^{\rm max}_{\rm er}$ and the optimal excitation energy $E^*_{\rm opt}$ dependence on θ_2. The corresponding graphs for the reaction ^{48}Ca + ^{238}U are shown in Figs. 6(a) and 6(b). From Fig. 6(a) one can see that $\sigma^{\rm max}_{\rm er}$ for both the $3n$ and $4n$ channels decreases with the increasing value of θ_2. Figure 6(b) shows that $E^*_{\rm opt}$ increases with increasing θ_2 for both the $3n$ and the $4n$ channels, and the discrepancy of the optimal excitation energy between the $3n$ and the $4n$ channels decreases with the increasing value of θ_2. In Fig. 6(a) it can be seen that the curve of the $3n$ channel is steeper than that of the $4n$ channel. This is probably because the optimal excitation energies of the $3n$ channel is lower than that of the $4n$ channel as shown in Fig. 6(b), and the capture cross section is more sensitive to the value of θ_2 at lower incident energies.

B. Production cross sections of isotopes with $Z = 113$–118 in ^{48}Ca-induced reactions

The production cross sections for the reactions ^{48}Ca + ^{237}Np, ^{243}Am, ^{244}Pu, ^{248}Cm, ^{249}Bk, and ^{249}Cf to produce elements $Z = 113 - 118$ are shown in Fig. 7. The shown curves represent the average results for different orientations of targets. There are no other adjustable parameters in the calculations. Within the error bars, the experimental data [3–10] are reproduced rather well except for the $3n$ channel

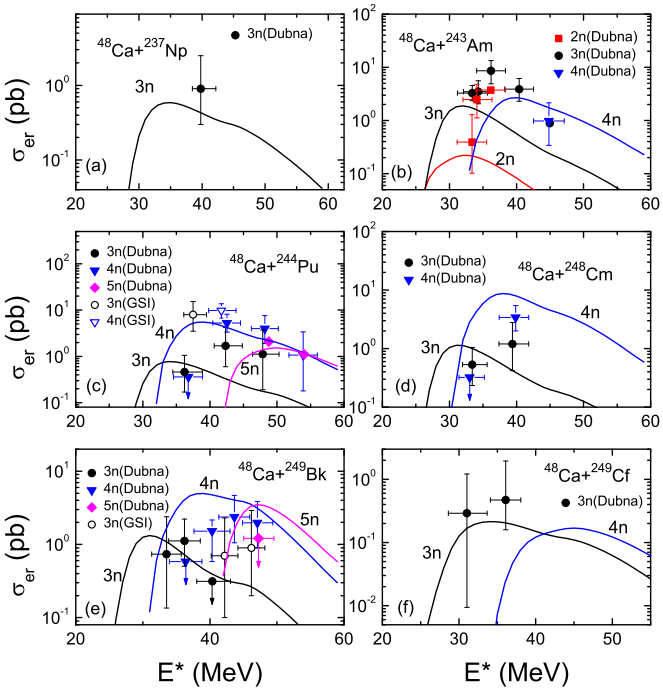

FIG. 7. (Color online) Comparison of calculated ER cross sections with the available experimental data for the reactions ^{48}Ca + ^{237}Np [7], ^{243}Am [4], ^{244}Pu [3,10], ^{248}Cm [6], ^{249}Bk [8,9], and ^{249}Cf [5] to produce elements Z = 113–118.

in the reaction ^{48}Ca + ^{243}Am. From Fig. 7(c) one can see the experimental data from GSI [10] are larger than the calculated values, especially for the 3n channel. However, the obtained results are in good agreement with the experimental data from Dubna [3]. Therefore, it is reasonable to calculate the production cross sections of SHN by averaging ER cross sections for different orientations of deformed nuclei. We predict the maximal ER cross section of the 4n channel in the reaction ^{48}Ca + ^{249}Cf to be 0.17 pb and the corresponding optimal excitation energy to be 45 MeV.

C. Production cross sections of Z = 119 and 120

Figure 8(a) shows the dependence of fusion probabilities on excitation energies ($J = 0$) for $\theta_2 = 0°$, 45°, and 90° in the reaction ^{48}Ca + ^{252}Es. One can see behavior similar to that of the reaction ^{48}Ca + ^{238}U shown in Fig. 5(b). Figure 8(b) shows the ER cross sections of the reaction ^{48}Ca + ^{252}Es for producing the superheavy element Z = 119. The solid and the dashed lines denote the ER cross sections of the 3n and the 4n channels, respectively. The results for $\theta_2 = 0°$, 45°, and 90° are also shown. Behavior similar to that shown in Fig. 6 with respect to the orientation effects of the maximal ER cross sections and the optimal excitation energies can be seen, while the maximal ER cross sections of the 4n channel increases with increasing θ_2. This is probably because the fusion probabilities increase strongly with increasing θ_2 and the orientation effects of the fusion probability play a predominant role in the corresponding optimal excitation energies. The thick solid lines and the thick dashed lines are

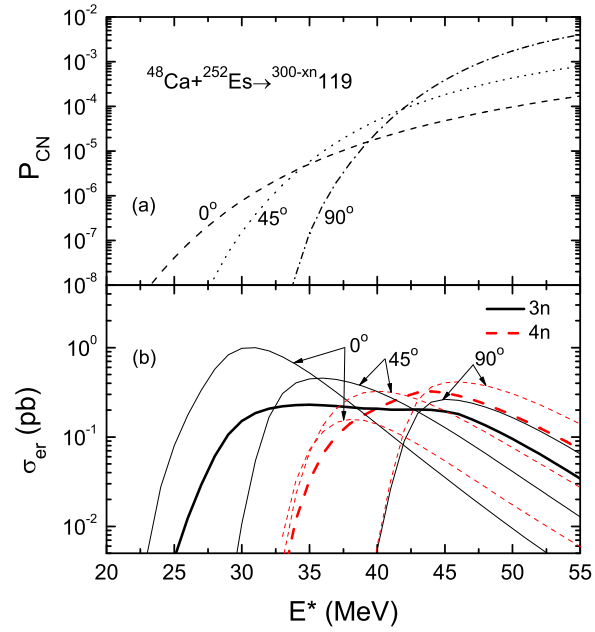

FIG. 8. (Color online) (a) Dependence of the fusion probability on excitation energies ($J = 0$) and θ_2 in the reaction ^{48}Ca + ^{252}Es → $^{(300-xn)}$119. (b) ER cross sections as a function of the excitation energy for the reaction ^{48}Ca + ^{252}Es. The solid lines and the dashed lines denote the calculated ER cross sections in the 3n and the 4n channels, respectively. The thick solid lines and the thick dashed lines denote the averaged results.

the average results for different values of θ_2. The average maximal ER cross sections of the 3n and the 4n channels are 0.23 and 0.32 pb, respectively. The results from Refs. [14,23] are of the same order of magnitude.

The fusion probabilities and ER cross sections of the reaction ^{48}Ca + ^{257}Fm → $^{(305-xn)}$120 are shown in Figs. 9(a)

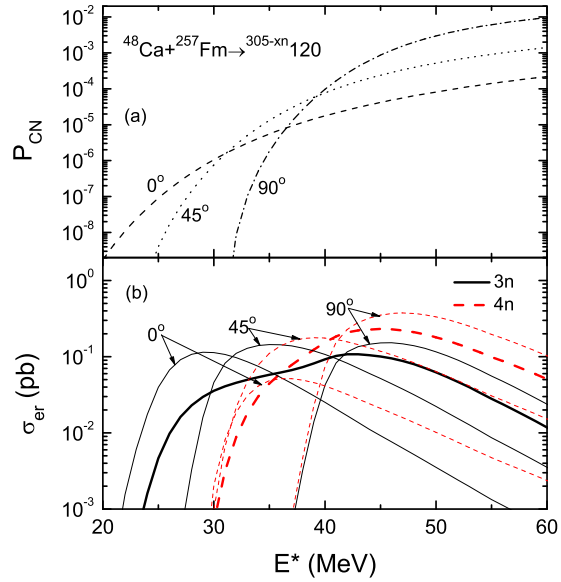

FIG. 9. (Color online) The same as in Fig. 8, but for the reaction ^{48}Ca + ^{257}Fm → $^{(305-xn)}$120.

and 9(b), respectively. The influence of θ_2 on P_{CN} shows behavior similar to that of other reactions. The average maximal ER cross sections of $3n$ and the $4n$ channels are 0.11 and 0.23 pb, respectively, which are quite reachable at available setups. From some theoretical predictions [14,15,41], it can be found that the production cross sections for producing $Z = 120$ in the reactions ^{50}Ti + ^{249}Cf and ^{54}Cm + ^{248}Cm are on the order of femtobarns, which seems to be beyond the limit of the available facilities. Therefore, the reaction ^{48}Ca + ^{257}Fm can be a better choice for synthesizing the superheavy element $Z = 120$ if enough ^{257}Fm can be collected to make a target. The ER cross sections for $\theta_2 = 0°$, 45°, and 90° are also shown. It can be seen that the orientation effects of the maximal ER cross sections of the $3n$ channel are not obvious. This is probably because the orientation effects of the fusion probabilities counteract those of the capture cross sections.

IV. CONCLUSIONS

In summary, within theframework of the DNS model, the orientation effects of the ER cross sections for the ^{48}Ca-induced hot fusion reactions are investigated. It is found that the orientation of colliding nuclei plays a significant role in fusion reactions. The effects of orientation on the fusion barrier, the capture cross sections, the fusion probability, the maximal ER cross sections, and the optimal excitation energies in the reaction ^{48}Ca + ^{238}U are investigated. The capture cross sections for $\theta_2 = 90°$ are obviously suppressed, especially at sub-barrier energies. According to the DNS concept, the fusion probability strongly depends on the inner fusion barrier, the QF barrier, and the excitation energy of the DNS. It is found that the fusion probabilities for $\theta_2 = 0°$ are much higher than those for $\theta_2 = 90°$ at lower incident energies, while the opposite behavior can be seen in the high incident energy region. The calculated average ER cross sections for different θ_2 are in good agreement with the experimental data.

It is reasonable to calculate the production cross sections of SHN by averaging ER cross sections for different orientations of deformed nuclei. The production cross sections of Z =119 and 120 through the reactions ^{48}Ca + ^{252}Es and ^{48}Ca + ^{257}Fm are predicted. The maximal production cross sections of Z =119 and 120 are 0.32 and 0.23 pb, respectively, in the $4n$ emission channel. In the future, if it will be possible to prepare targets of ^{252}Es and ^{257}Fm, and then the superheavy elements Z =119 and 120 probably can be synthesized.

ACKNOWLEDGMENTS

This work was supported by the National Natural Science Foundation of China under Grants No. 11025524 and No. 11161130520, the National Basic Research Program of China under Grant No. 2010CB832903, and the European Commission's 7th Framework Programme (FP7-PEOPLE-2010-IRSES) under Grant Agreement Project No. 269131.

[1] S. Hofmann and G. Münzenberg, Rev. Mod. Phys. **72**, 733 (2000); S. Hofmann, F. P. Heßberger, D. Ackermann, G. Münzenberg, S. Antalic, P. Cagarda, B. Kindler, J. Kojouharova, M. Leino, B. Lommel, R. Mann, A. G. Popeko, S. Reshitko, S. Śaro, J. Uusitalo, and A. V. Yeremin, Eur. Phys. J. A **14**, 147 (2002).
[2] K. Morita *et al.*, J. Phys. Soc. Jpn. **81**, 103201 (2012).
[3] Yu. Ts. Oganessian *et al.*, Phys. Rev. C **69**, 054607 (2004).
[4] Yu. Ts. Oganessian *et al.*, Phys. Rev. C **87**, 014302 (2013).
[5] Yu. Ts. Oganessian *et al.*, Phys. Rev. C **74**, 044602 (2006).
[6] Yu. Ts. Oganessian *et al.*, Phys. Rev. C **70**, 064609 (2004).
[7] Yu. Ts. Oganessian *et al.*, Phys. Rev. C **76**, 011601(R) (2007).
[8] Yu. Ts. Oganessian *et al.*, Phys. Rev. C **87**, 054621 (2013).
[9] J. Khuyagbaatar *et al.*, Phys. Rev. Lett. **112**, 172501 (2014).
[10] Ch. E. Düllmann *et al.*, Phys. Rev. Lett. **104**, 252701 (2010).
[11] G. G. Adamian, N. V. Antonenko, W. Scheid, and V. V. Volkov, Nucl. Phys. A **627**, 361 (1997).
[12] N. Wang, E.-G. Zhao, W. Scheid, and S.-G. Zhou, Phys. Rev. C **85**, 041601(R) (2012).
[13] Y. Abe, D. Boilley, B. Giraud, G. Kosenko, and C. Shen, Acta Phys. Hung. A **19**, 77 (2004).
[14] L. Zhu, W. J. Xie, and F. S. Zhang, Phys. Rev. C **89**, 024615 (2014).
[15] Z. H. Liu and J. D. Bao, Phys. Rev. C **89**, 024604 (2014).
[16] K. Siwek-Wilczyńska, T. Cap, M. Kowal, A. Sobiczewski, and J. Wilczyński, Phys. Rev. C **86**, 014611 (2012).
[17] C. W. Shen, Y. Abe, D. Boilley, G. Kosenko, and E. G. Zhao, Int. J. Mod. Phys. E **17**, 66 (2008).
[18] G. Mandaglio, G. Giardina, A. K. Nasirov, and A. Sobiczewski, Phys. Rev. C **86**, 064607 (2012).
[19] R. Smolańczuk, Phys. Rev. C **81**, 067602 (2010).
[20] V. I. Zagrebaev, Phys. Rev. C **64**, 034606 (2001).
[21] Y. Abe, A. Marchix, C. Shen, B. Yilmaz, G. Kosenko, D. Boilley, and B. G. Giraud, Int. J. Mod. Phys. E **16**, 491 (2007).
[22] Z. Q. Feng, G. M. Jin, J. Q. Li, and W. Scheid, Phys. Rev. C **76**, 044606 (2007).
[23] M. H. Huang, Z. G. Gan, X. H. Zhou, J. Q. Li, and W. Scheid, Phys. Rev. C **82**, 044614 (2010).
[24] G. G. Adamian, N. V. Antonenko, and W. Scheid, Phys. Rev. C **68**, 034601 (2003).
[25] G. G. Adamian, N. V. Antonenko, and W. Scheid, Phys. Rev. C **69**, 011601(R) (2004).
[26] Z. Q. Feng, G. M. Jin, F. Fu, and J. Q. Li, Nucl. Phys. A **771**, 50 (2006).
[27] G. G. Adamian, N. V. Antonenko, W. Scheid, and V. V. Volkov, Nucl. Phys. A **633**, 409 (1998).
[28] G. G. Adamian, N. V. Antonenko, and W. Scheid, Phys. Rev. C **69**, 014607 (2004); **69**, 044601 (2004).
[29] G. G. Adamian, N. V. Antonenko, and W. Scheid, Nucl. Phys. A **678**, 24 (2000).
[30] V. Zagrebaev and W. Greiner, Phys. Rev. C **78**, 034610 (2008).
[31] K. Nishio, S. Mitsuoka, I. Nishinaka, H. Makii, Y. Wakabayashi, H. Ikezoe, K. Hirose, T. Ohtsuki, Y. Aritomo, and S. Hofmann, Phys. Rev. C **86**, 034608 (2012).
[32] K. Nishio, H. Ikezoe, S. Mitsuoka, I. Nishinaka, Y. Nagame, Y. Watanabe, T. Ohtsuki, K. Hirose, and S. Hofmann, Phys. Rev. C **77**, 064607 (2008).

[33] L. Zhu, J. Su, W. J. Xie, and F. S. Zhang, Nucl. Phys. A **915**, 90 (2013).
[34] Yu. Ts. Oganessian, J. Phys. G **34**, R165 (2007).
[35] P. Reiter *et al.*, Phys. Rev. Lett. **82**, 509 (1999).
[36] J. R. Leigh, M. Dasgupta, D. J. Hinde, J. C. Mein, C. R. Morton, R. C. Lemmon, J. P. Lestone, J. O. Newton, H. Timmers, J. X. Wei, and N. Rowley, Phys. Rev. C **52**, 3151 (1995).
[37] C. Y. Wong, Phys. Rev. Lett. **31**, 766 (1973).
[38] P. Möller, J. R. Nix, W. D. Myers, and W. J. Swiatecki, At. Data Nucl. Data Tables **59**, 185 (1995).
[39] G. Wolschin and W. Nörenberg, Z. Phys. A **284**, 209 (1978).
[40] M. G. Itkis *et al.*, J. Nucl. Radiochem. Sci. **3**, 57 (2002).
[41] N. Wang, J. L. Tian, and W. Scheid, Phys. Rev. C **84**, 061601(R) (2011).